The Astrophysical Journal, 599:24–30, 2003 December 10

MODELING DYNAMICAL DARK ENERGY

R. Mainini, A. V. Macciò, and S. A. Bonometto
Physics Department G. Occhialini, Università degli Studi di Milano-Bicocca, Piazza della Scienza 3, I-20126 Milan, Italy; and INFN, Via Celoria 16, I-20133 Milan, Italy

and

A. Klypin
Astronomy Department, Box 30001, Department 4500, New Mexico State University, Las Cruces, NM 88003-0001
Received 2003 March 13; accepted 2003 June 24

ABSTRACT

Cosmological models with different types of dark energy are becoming viable alternatives for standard models with the cosmological constant, yet such models are more difficult to analyze and to simulate. We present analytical approximations and discuss ways of making simulations for two families of models, which cover a wide range of possibilities and include models with both slow- and fast-changing ratio $w = p/\rho$. More specifically, we give analytical expressions for the evolution of the matter density parameter $\Omega_m(z)$ and the virial density contrast Δ_c at any redshift z. The latter is used to identify halos and to find their virial masses. We also provide an approximation for the linear growth factor of linear fluctuations between redshift $z = 40$ and 0. This is needed to set the normalization of the spectrum of fluctuations. Finally, we discuss the expected behavior of the halo mass function and its time evolution.

Subject headings: cosmology: theory — dark matter — galaxies: clusters: general — methods: analytical — methods: numerical

1. INTRODUCTION

Observations of high-redshift supernovae (Perlmutter et al. 1999; Riess et al. 1998), as well as the analysis of fluctuations of the cosmic microwave background combined with data on the large-scale structure of galactic distribution (e.g., Balbi et al. 2000; Tegmark, Zaldarriaga, & Hamilton 2001; Netterfield et al. 2002; Pogosyan, Bond, & Contaldi 2003; Spergel et al. 2003), indicate that there is a significant component of smooth energy with large negative pressure, characterized by a parameter $w \equiv p/\rho \lesssim -0.5$. This component is dubbed dark energy (DE). The nature of DE is open for debate, with candidates ranging from a cosmological constant Λ to a slowly evolving scalar field ϕ to even more exotic physics of extra dimensions (e.g., Dvali & Turner 2003).

One of the most appealing ideas for DE is a self-interacting scalar field, which evolves with time (Ratra & Peebles 1988, hereafter RP; Wetterich 1988). We call this dynamical DE. The advantage of the dynamical DE models as compared to the Λ-dominated cold dark matter (ΛCDM) models is that DE naturally yields an accelerated expansion, easing the problem of fine tuning. The observational signatures of dynamical DE should be carefully investigated in order to determine which measures can be used to discriminate ΛCDM from dynamical DE and among different dynamical DE models. In this paper we focus on the two most popular variants of dynamical DE. RP studied DE models, which cause a rather slow evolution of w. Models based on simple potentials in supergravity (SUGRA) result in a faster evolving w (Brax & Martin 1999, 2000). Together, RP and SUGRA potentials cover a large spectrum of evolving w. The potentials are written as

$$V(\phi) = \frac{\Lambda^{4+\alpha}}{\phi^\alpha} \ (\mathrm{RP}) \ , \tag{1}$$

$$V(\phi) = \frac{\Lambda^{4+\alpha}}{\phi^\alpha} \exp\left(4\pi G\phi^2\right) \ (\mathrm{SUGRA}) \ . \tag{2}$$

Here Λ is an energy scale, currently set in the range 10^2–10^{10} GeV, relevant for fundamental interaction physics. The potentials depend also on the exponent α. Once the parameters Λ and α are assigned, the DE density parameter Ω_{DE} follows. Here, however, we prefer to use Λ and Ω_{DE} as independent parameters.

Dynamical DE has kinetic and potential components, $\dot{\phi}^2/2$ and $V(\phi)$, respectively. Those factors define the energy density ρ_{DE} and the pressure p_{DE}. In general, the ratio of the pressure and the density,

$$w = \frac{p_{\mathrm{DE}}}{\rho_{\mathrm{DE}}} = \frac{\dot{\phi}^2/2 - V(\phi)}{\dot{\phi}^2/2 + V(\phi)} \ , \tag{3}$$

changes with time and is typically negative when the potential V is sufficiently large, as one expects to occur in the recent epoch.

In order to simplify the situation, the dynamical DE is often replaced with models with constant $w \neq -1$. This can be considered as a formal generalization of the equation of state of vacuum energy density for which $w \equiv -1$. These models result in accelerated expansion if w exceeds $\approx -\frac{1}{3}$. The main advantage of constant w is to yield models easier to deal with than the dynamical DE. Although finding a physical justification for models with constant $w \neq -1$ is more difficult than for the cosmological constant (see, however, Caldwell 2002), these models are still useful as toy models, allowing one to inspect the effects of an acceleration that is slower than with the vacuum energy (for a recent review, see Peebles & Ratra 2003).

In this paper we show how complications with the dynamical DE can be overcome if one uses suitable approximations, which we provide. Besides allowing an easier treatment of the dynamical DE, these expressions also allow us to compare the dynamical DE with the models with constant w. One of the results of this comparison is that differences between constant w and dynamical DE are significant, being comparable to those between ΛCDM and constant w (differences between constant and variable w can be important also when data concern a narrower redshift range; then they are not of the same order as those with ΛCDM, but in spite of that, neglecting them can cause a significant bias; an example is the analysis of Type Ia supernova data performed by Podariu & Ratra 2000).

The results given in this paper are based on a modified version of the CMBFAST code. The modifications include effects due to the change in the rate of the expansion of the universe and fluctuations of the scalar field. Although these fluctuations rapidly fade, soon after they enter the horizon, their effect on cosmic microwave background anisotropies and polarization is quite significant, while they also cause (smaller) modifications to the transfer function on large scales.

In addition, we also estimate the growth of linear and nonlinear fluctuations of nonrelativistic matter only. Previously, our algorithms were used by Mainini, Macciò, & Bonometto (2003, hereafter MMB03).

Making use of these algorithms, in this paper we work out (1) analytical approximations of the dependence of the matter density parameter Ω_m on the redshift z, (2) modifications to run N-body simulations of the clustering of dynamical DE models, and (3) analytical approximations for the virial density contrast Δ_c at any redshift z. Expressions derived from the linear theory can also be used to compare the observables deduced for dynamical DE and for constant w. We argue that these approximations make an analysis of the dynamical DE as simple as for models with constant w.

2. THE VIRIAL DENSITY CONTRAST

We start with finding the evolution of the density contrast in the top-hat approximation for models with DE. Considering a spherical fluctuation greatly simplifies the analytical and numerical treatment of the nonlinear problem. Much work has been done in this line, starting with Gunn & Gott (1972), Gott & Rees (1975), and Peebles (1980), who studied the spherical collapse in standard CDM (SCDM) models. Lahav et al. (1991), Eke, Cole, & Frenk (1996), Brian & Norman (1998), and others generalized the results to the case of ΛCDM. If the initial density contrast of a spherical perturbation is $\Delta_i = 1 + \delta_i$, and its initial radius is R_i, then the radius of the perturbation $R = rR_i$ at later times can be found using the equation

$$\frac{\ddot{r}}{r} = -H_i^2\left[\frac{\Omega_{m,i}\Delta_i}{2r^3} + \Omega_{r,i}\left(\frac{a_i}{a}\right)^4 + \frac{(1+3w)\rho_{\rm DE}}{2\rho_{{\rm cr},i}}\right] , \quad (4)$$

where all quantities with subscript i refer to the initial time. In particular, $\Omega_{m,i}$ and $\Omega_{r,i}$ are the density parameters for nonrelativistic and relativistic matter at that time. To integrate this equation, the time dependence of $\rho_{\rm DE}$ and w must also be worked out (see eq. [3]). In turn, this requires the integration of the equation of motion

$$\ddot{\phi} + 3\left(\frac{\dot{a}}{a}\right)\dot{\phi} + \frac{\partial V}{\partial \phi} = 0 , \quad (5)$$

yielding ϕ and $\dot{\phi}$ to be used in equation (3), and the Friedmann equation, yielding $\dot{a}/a$ (see also § 4 here below). Initial conditions to solve equation (5) are set in the radiation-dominated era, using the tracker solution. After slowing down relative to the scale factor $a(t)$, the perturbation eventually stops at turnaround time $t_{\rm ta}$, when its radius is $R_{\rm ta}$. The radius R formally goes to zero at $\sim 2t_{\rm ta}$, corresponding to redshift $z_{\rm col}$. The value of $z_{\rm col}$ depends on the amplitude of the initial fluctuation δ_i. Instead of δ_i, it is, however, convenient to use the amplitude δ_c as estimated by the linear theory at $z_{\rm col}$. For SCDM the value of this density contrast is

$$\delta_c^* \simeq 1.68 \quad (6)$$

and does not depend on $z_{\rm col}$ (see, e.g., Coles & Lucchin 1995). For other models, δ_c does depend on $z_{\rm col}$.

In the contraction stages fluctuations heat up, and unless kinetic energy can be successfully radiated away, contraction will stop when virial equilibrium is attained and its size is R_v. Requiring energy conservation and virial equilibrium, we obtain the algebraic cubic equation

$$x^3 - \frac{1 + y(a_{\rm ta})}{2y(a_{\rm col})}x + \frac{1}{4y(a_{\rm col})} = 0 , \quad (7)$$

where $x = R_v/R_{\rm ta}$ and

$$y(a) = \frac{1 - \Omega_m(a)}{\Delta_i\Omega_m(a)}\left(\frac{R_{\rm ta}}{R_i}\right)^3\left(\frac{a_i}{a}\right)^3 . \quad (8)$$

Note that the actual radius of the final virialized halo is often larger than R_v, owing to deviations from spherical growth in the real world (Macciò, Murante, & Bonometto 2003). Still, R_v is a good starting point for statistical analysis. Multiplying equation (7) by $2y$ and then taking $y = 0$ (i.e., $\Omega_m \equiv 1$: SCDM), we recover $x = \frac{1}{2}$. In general, the root x lies slightly below this value.

Figure 1 shows the linear and nonlinear growth of a density contrast for SCDM, ΛCDM, and RP models normalized to have $z_{\rm col} = 0$. Similar plots can be made for any redshift of collapse. The figure can be used to find the initial amplitude Δ_i at any given redshift z_i and the value of δ_c for a perturbation collapsing at present.

Using the final value of Δ, we obtain the virial density contrast:

$$\Delta_c = \Omega_m\Delta . \quad (9)$$

In the linear and nonlinear cases, deviations from the SCDM behavior often compensate each other, and the final values of δ_c are just slightly model-dependent (see Fig. 2 and MMB03 for more details). The spread among the virial density contrasts, Δ_c, is large, as indicated by Figure 3, which shows Δ_c as a function of Ω_m for different models. The evolution of Δ_c with redshift is also very model-dependent, as shown by Figure 4. We provide an approximation, which is valid at any redshift z, provided that we know the matter density parameter Ω_m at that redshift:

$$\Delta_c = 178(\Omega_m)^{\mu(\Omega_m,\,\Lambda)} . \quad (10)$$

Here $\mu(\Omega_m,\ \Lambda) = a + b(\Omega_m)^c$ with $c = 1$ for RP and 2 for SUGRA. Parameters a and b are given by

$$a = a_1\lambda + a_2 , \quad b = b_1\lambda + b_2 , \quad (11)$$

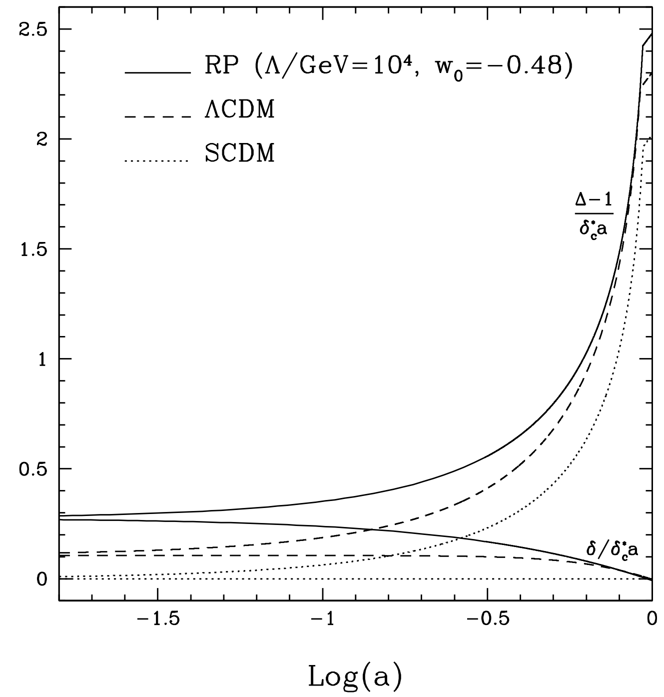

FIG. 1.—Normalized linear (*bottom curves*) and nonlinear (*top curves*) amplitude of density fluctuations for SCDM (*dotted curves*), ΛCDM (*dashed curves*), and RP (*solid curves*) models. The amplitude of fluctuation was normalized to collapse the perturbation at $z_{\rm col} = 0$. Similar plots can be given for a collapse at any other redshift. The density contrast $\Delta = \Delta_c/\Omega_m$, and w_0 is the value of w at $z = 0$.

where

$$\lambda = \log(\Lambda/{\rm GeV}) \quad (12)$$

and the coefficients are given in Table 1.

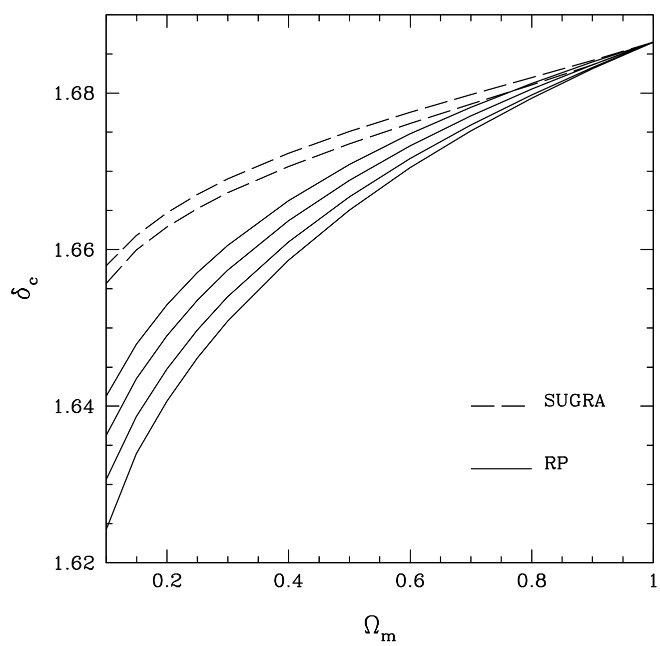

FIG. 2.—Dependence of δ_c on the matter density parameter Ω_m at $z = 0$ for four RP ($\Lambda/{\rm GeV} = 10^2$, 10^4, 10^6, and 10^8) and two SUGRA models ($\Lambda/{\rm GeV} = 10^2$ and 10^8). The value of Λ increases from the top to the bottom curves.

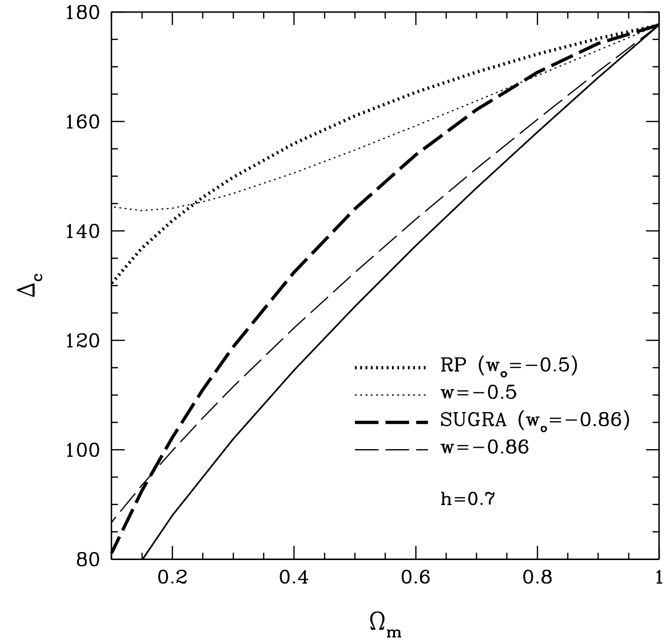

FIG. 3.—Dependence of Ω_m on Δ_c for different cosmologies. The RP and SUGRA models, at $z = 0$, have a pressure/density ratio $w_0 = w$ for the constant-w models shown. The solid curve is for ΛCDM.

Figure 5 shows the dependence on λ of the differences $|\Delta_c^{\rm num}/\Delta_c^{\rm an} - 1|$ at $z = 0$, for models with $h = 0.7$ and different values of λ, as a function of Ω_m. (Here $\Delta_c^{\rm num}$ is obtained from the full numerical treatment, while $\Delta_c^{\rm an}$ is the expression [10].) Discrepancies stay below 0.5% for any $\Omega_m \lesssim 0.15$. However, for large λ, the approximation is even better: $\lesssim 0.2$% for any Ω_m.

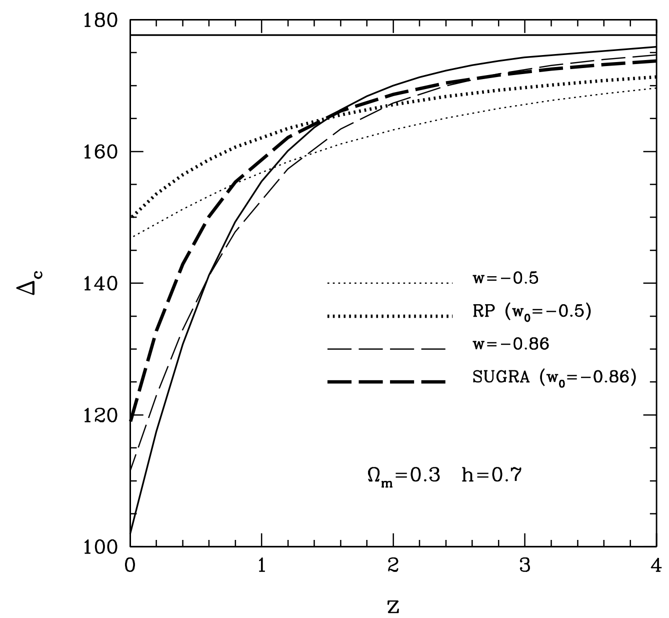

FIG. 4.—Redshift dependence of Δ_c for different cosmologies. The RP and SUGRA models, at $z = 0$, have a pressure/density ratio $w_0 = w$ for the constant-w models shown. The solid curves are for SCDM (*upper horizontal line*) and ΛCDM.

TABLE 1
INTERPOLATION COEFFICIENTS FOR Δ_c

Model	a_1	a_2	b_1	b_2
RP	-1.45×10^{-2}	0.186	-0.011	0.22
SUGRA..........	-2.25×10^{-3}	0.3545	-0.01875	-0.1225

3. THE MASS FUNCTION AND THE LINEAR GROWTH FACTORS FOR DYNAMICAL DE

We use both the Press-Schechter (1974, hereafter PS) and the Sheth-Tormen (1999, 2002, hereafter ST) approximations for the mass function of dark matter halos. The value of δ_c defines the bias factor $\nu = \delta_c/\sigma_M$ for the mass M. Here σ_M is the rms density fluctuation on this scale. The bias factor then enters the expression

$$f(\nu)\nu\, d\log\nu = \frac{M}{\rho_m} n_h(M) M\, d\log M\ , \qquad (13)$$

with either

$$f(\nu)\nu = \sqrt{\frac{2}{\pi}}\nu\exp\left(-\frac{\nu^2}{2}\right)\ (\mathrm{PS})\ , \qquad (14)$$

or

$$f(\nu)\nu = A\left[1 + (\nu')^{-2q}\right]\sqrt{\frac{2}{\pi}}\nu'\exp\left[\frac{-(\nu')^2}{2}\right]\ (\mathrm{ST})\ , \qquad (15)$$

with a small complication in the ST case: here $\nu' = \sqrt{a}\nu$ with $a = 0.707$, while the constants $q = 0.3$ and $A = 0.3222$. Using equation (13) we obtain the differential mass function $n_h(M)$ in the PS and ST approximations, once the distribution on bias is given. Here, as usual, we assume a Gaussian $f(\nu)$. Equations (13)–(15) can then be integrated to obtain the halo mass function $n_h(> M,\ z)$ at any redshift z.

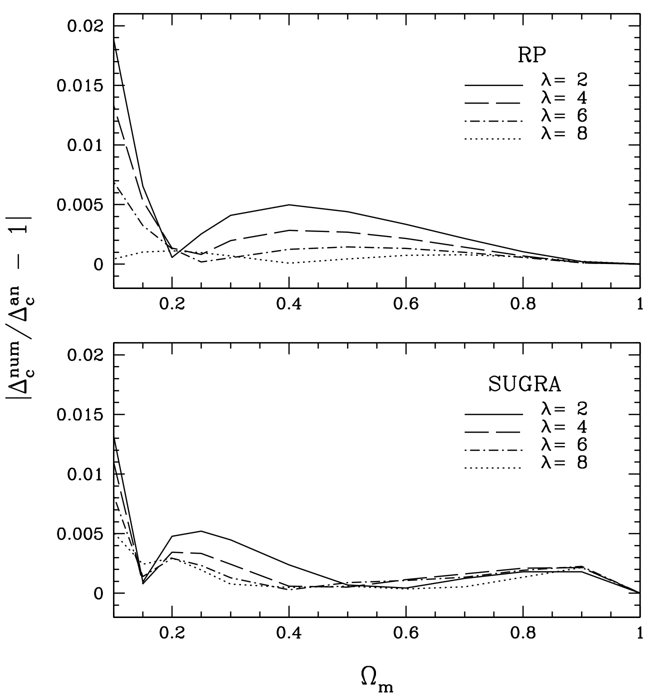

FIG. 5.—Fractional discrepancy between numerical and analytical results on Δ_c.

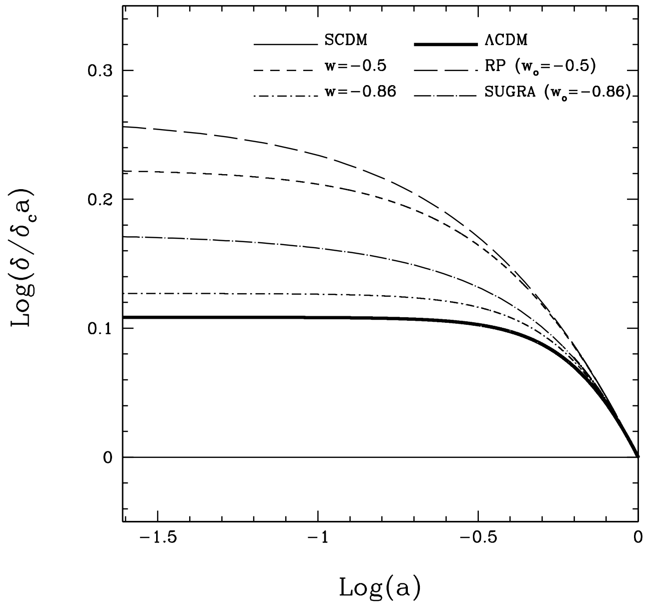

FIG. 6.—Linear growth factor for various models

Such a computation must use appropriate values for δ_c and σ_M; the latter are computed by integrating the power spectrum $P(k)$. Its shape depends on the specific choice of dynamical DE, as our modified CMBFAST program shows. However, the dependence is very mild for wavelengths smaller than the galaxy cluster scale. On the contrary, as can be seen also from Figure 1, the linear growth factor depends on the DE nature in quite a significant way. Figure 6 presents the z-dependence of the growth factor for z up to 40 and for a number of different models.

In particular, Figure 6 shows that at redshift $z \geq 2$ the difference between ΛCDM and a model with constant $w = -0.86$ is equal to or even smaller than the very difference between this constant-w model and the SUGRA model, yielding the same ratio w at $z = 0$. However, the latter difference becomes comparable to the former one already at $z \gtrsim 0.5$. A constant-w approximation seems to perform better for RP models, but this can be mostly ascribed to the fact that the ratio w at $z = 0$ is smaller for these models. Their distance from ΛCDM is therefore greater, and the difference between them and constant-w models appears comparatively smaller. However, also in this case, using constant w instead of RP at $z \geq 4$ is surely misleading.

The linear growth factor shown in Figure 6 is very important for setting the initial conditions of N-body simulations because linear growth factors are required for the normalization of the power spectrum at the initial redshift $z_{\rm in}$ of simulations. For these reasons we also give an analytical approximation that reproduces fairly well the behavior of the linear growth factors at $z = 40$ for different values of $\Omega_m(z = 0)$ and λ:

$$\frac{\delta_c}{\delta(z = 40)} = A + B\lambda + C\lambda^2\ . \qquad (16)$$

The values of the coefficients A, B, and C are presented in Table 2 for the RP and SUGRA models, respectively. At

TABLE 2
COEFFICIENTS FOR THE LINEAR GROWTH FACTOR

Parameter	$\Omega_m = 0.2$	$\Omega_m = 0.3$	$\Omega_m = 0.4$
SUGRA			
A	25.6	28.5	30.7
B	−0.237	−0.26	−0.274
C	0	0	0
RP			
A	21.3	25.1	28.2
B	−0.755	−0.783	−0.698
C	−0.0125	−0.0155	−0.0155

TABLE 3
COEFFICIENTS FOR $\Omega_m(z)$

Parameter	$\Omega_m = 0.2$	$\Omega_m = 0.3$	$\Omega_m = 0.4$
RP			
a_1	-5.638×10^{-3}	-2.119×10^{-2}	-3.365×10^{-2}
a_2	−0.813	−0.259	0.207
b_1	-2.460×10^{-2}	-1.833×10^{-2}	-1.384×10^{-2}
b_2	1.382	0.975	0.628
c_1	-5.960×10^{-3}	-6.975×10^{-3}	-8.394×10^{-3}
c_2	8.460×10^{-2}	9.771×10^{-2}	0.119
SUGRA			
a_1	-8.466×10^{-3}	-9.161×10^{-3}	-2.035×10^{-2}
a_2	1.383	1.415	1.427
b_1	-1.386×10^{-2}	-1.753×10^{-2}	-1.336×10^{-2}
b_2	-8.521×10^{-3}	-6.890×10^{-3}	-1.289×10^{-2}
c_1	-3.935×10^{-2}	-4.421×10^{-2}	-4.203×10^{-2}
c_2	0.710	0.688	0.682
d_1	2.088×10^{-2}	1.875×10^{-2}	2.212×10^{-2}
d_2	−0.883	−0.621	−0.416

$z = 40$, the discrepancies between Ω_m and unity already range around 2%–3%. If a simulation must be started at larger z, extrapolating the linear growth factor by assuming that $\delta \propto a$ at $z > 40$ implies an error smaller than such a percentage. This can still be improved by assuming that $\delta \propto a^{\Omega_m^q}$, with $q \simeq 0.4$. The dependence of q on the model and on the energy scale λ fixes the second decimal of q and allows a precision better than 0.01%, which is out of the scope of this analysis.

Mass functions $n(>M,\ z)$, obtained according to equations (13)–(15), are compared with simulations in the accompanying paper (Klypin et al. 2003). Similar mass functions, obtained from the PS expressions, were used in MMB03 to estimate the expected observable differences between models with different dynamical DE.

4. EVOLUTION OF THE MATTER DENSITY PARAMETER

In the RP and SUGRA models, at variance from models with $w = \text{const}$, no analytical expression of $\Omega_m(a)$ is readily available. An accurate approximate expression of Ω_m for various redshifts and for different models is useful for various purposes. In particular, it can be used in conjunction with equations (10) and (11) to find the value of Δ_c at $z \neq 0$.

We found the following fitting formula:

$$\Omega_m(a) = 1 - \frac{1 - \Omega_{m,0}}{(1+z)^{\alpha(z,\lambda)}} , \qquad (17)$$

where $\Omega_{m,0}$ is the matter density parameter at $z = 0$, while $\alpha(z,\ \lambda) = a + bz^c + d/(1+z)$ with $d = 0$ for the RP models. Parameters a, b, c, and d have the same structure as equation (11). The coefficients are given in Table 3.

Figure 7 shows the errors of approximation $|\Omega_m^{\rm num}/\Omega_m^{\rm an} - 1|$ as a function of the redshift z for two RP and two SUGRA models with $\Omega_m = 0.3$ and $h = 0.7$.

All that is needed to find the relation between the scale factor a and time in any flat dynamical DE model is such an expression. In fact, let us remember that

$$\frac{\dot{a}}{a} = H_0 \sqrt{\frac{\rho(a)}{\rho_{{\rm cr},0}}} , \qquad (18)$$

with

$$\rho(a) = \frac{\rho_{m,0}}{a^3} + \frac{\rho_{r,0}}{a^4} + \frac{\dot{\phi}^2}{2} + V(\phi) . \qquad (19)$$

At low z, we can omit the contribution of the radiation density. Therefore, at any time,

$$\rho_\phi = \frac{\dot{\phi}^2}{2} + V(\phi) = \rho_{\rm cr}(a)[1 - \Omega_m(a)] = \rho_m(a)\frac{1 - \Omega_m(a)}{\Omega_m(a)} , \qquad (20)$$

provided that we are dealing with a model such that the total density is equal to the critical density $\rho_{\rm cr}(a)$. Then, the

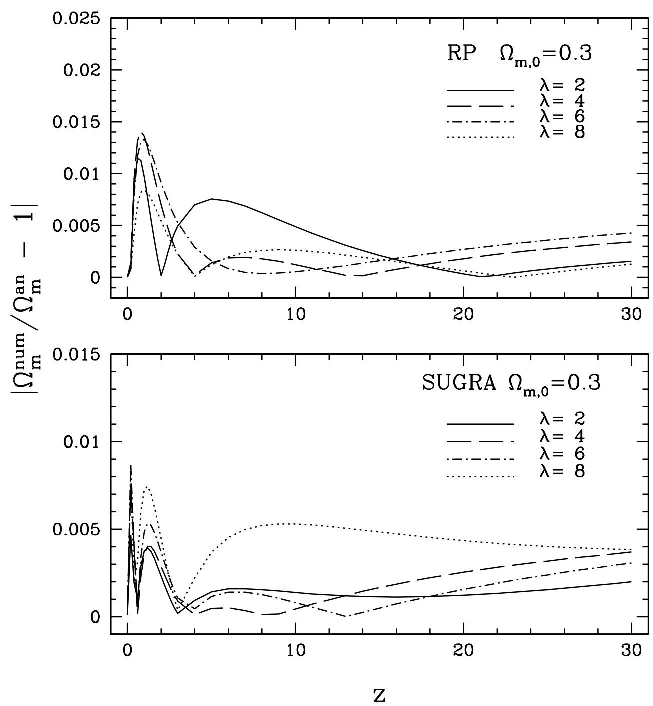

FIG. 7.—Fractional discrepancies between the approximated expression (17) and numerical data.

Friedmann equation reads

$$\left(\frac{\dot{a}}{a}\right)^2 = \frac{8\pi}{3} G\rho_m(a)\left[1 + \frac{1-\Omega_m(a)}{\Omega_m(a)}\right] = \frac{8\pi}{3} G \frac{\rho_{m,0}}{a^3\Omega_m(a)} , \quad (21)$$

so that

$$\frac{\dot{a}}{a} = H_0\sqrt{\frac{\Omega_{m,0}}{a^3\Omega_m(a)}} . \quad (22)$$

This formula is valid regardless of the equation of state of DE. In models with constant w, the density $\rho_{\rm DE} \propto a^{-3(1+w)}$, and therefore, owing to equation (21),

$$\Omega_m(a) = \left[1 + a^{-3w}\left(\Omega_{m,0}^{-1} - 1\right)\right]^{-1} . \quad (23)$$

Expressions (17)–(23), yielding $\Omega_m(a)$, as well as equation (22), yielding $\rho_{\rm cr}$, can be used in N-body programs to determine the trajectories of particles in an expanding universe. In fact, once we know Ω_m and $\rho_{\rm cr}$, we can integrate the Poisson equation $\nabla^2\Phi = -4\pi G a^2\rho_{\rm cr}\Omega_m\delta_m$, yielding the peculiar potential Φ due to the density fluctuations δ_m, obtained from the particle distribution. Then the equations of motion of each particle,

$$\frac{d\boldsymbol{p}}{da} = -\dot{a}\nabla_x\Phi , \quad \frac{d\boldsymbol{x}}{da} = \frac{\boldsymbol{p}}{a^2\dot{a}} \quad (24)$$

(see, e.g., Peebles 1980; here $\boldsymbol{p} \equiv a\boldsymbol{v}$), can be integrated using $\dot{a}$ given by equation (22), and we obtain the evolution of particle positions as a function of the scale factor a. The N-body Adaptive Refinement Tree (ART) code (Kravtsov, Klypin, & Khokhlov 1997), used in the accompanying paper (Klypin et al. 2003) to discuss the evolution of models with dynamical DE and DE with constant w, has been modified on these bases.

Figure 8 compares the expansion law $a_{\rm apx}(t)$, obtained using equations (17) and (18), with the numerical behavior $a_{\rm num}(t)$. Discrepancies seldom exceed 0.4% and are mostly well below 0.1%. For any practical purposes, the errors are negligible.

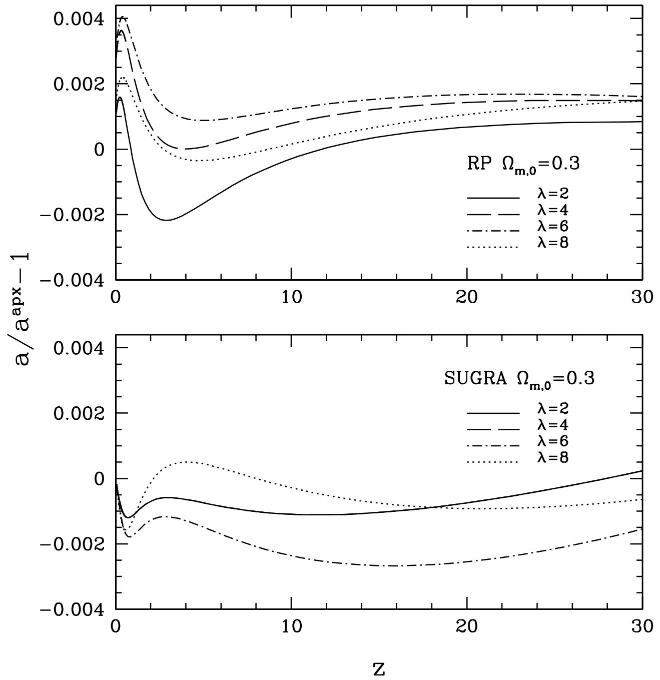

FIG. 8.—Fractional discrepancies between the analytical and numerical integrations of eq. (18) to obtain $a(t)$.

5. DISCUSSION

Observational effects of DE have been considered by various authors, but often models with a constant w are used. Besides being simpler, constant-w models give a feeling that results are generic in the sense that they do not depend on the nature of the underlying DE. For instance, Wang & Steinhardt (1998), Steinhardt, Zlatev, & Wang (1999), Zlatev, Wang, & Steinhardt (1999), and Lokas (2002) derived the Δ_c-dependence on Ω_m and w in the constant-w approximation. Schuecker et al. (2003) extended the results to large negative w-values to include the case of phantom energy (Caldwell 2002; Schulz & White 2001).

Unfortunately, results depend on what is assumed for the DE. Figure 3 shows the dependence of Δ_c on w for models with $\Omega_m = 0.3$ and $h = 0.7$ for three cases: DE as the cosmological constant, constant $w \neq -1$, and dynamical DE with RP or SUGRA potentials. The difference between constant w and dynamical DE is as large as the difference between ΛCDM and constant w. In other words, if we need to consider models more sophisticated than ΛCDM, it is not enough to discuss only constant $w \neq -1$. Figure 9 illustrates that the growth factor for dynamical DE cannot be approximated by a model with constant w. It seems clear that the universe "knows" the underlying physics, and predictions depend on the shape of the potential of the scalar field responsible for the DE.

In principle, finding astrophysical quantities that depend on microphysics is far from being unwelcome. Accordingly, the detailed dependence of astrophysical observables on microphysical parameters deserves to be inspected. Let us

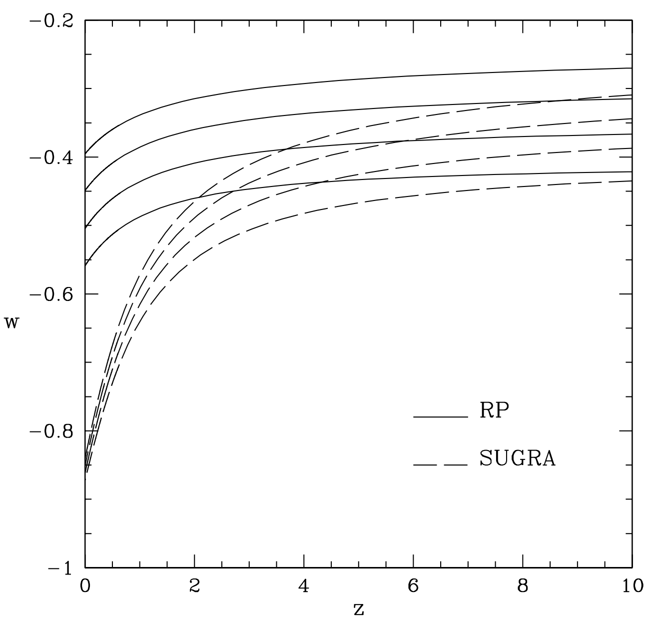

FIG. 9.—Redshift dependence of w for four RP and four SUGRA models ($\lambda = 1$, 3, 5, and 7); λ decreases from the top to the bottom curves.

outline, in particular, that Figure 3 applies to observations at $z = 0$, while the effects of dynamical DE are also expected at higher z. In fact, in Figure 4 we show the z-dependence of Δ_c for three sets of models characterized by the same values of w at $z = 0$. The figure shows that the differences between values of Δ_c increase from $z = 0$ toward intermediate redshifts, to go back to SCDM values at high redshifts, when ordinary matter gradually approaches critical density.

Intermediate redshifts, however, are the most relevant for present and future observations. Figure 10 shows that, at these redshifts, the dependence on the nature of DE arises from actual changes of w. Therefore, apart from any consideration concerning fundamental physics, Δ_c-values at high z obtained within the constant-w approximation risk the creation of bias.

Our aim is to facilitate the usage of dynamical DE. We provide the following tools: (1) an approximation for $\Omega_m(a)$, (2) an interpolating expression for Δ_c, valid at any redshift for given $\Omega_m(a)$, (3) an analytical expression for the rate of change of the expansion parameter needed for running N-body simulations and hydrosimulations, and (4) a plot of the linear growth factor, for a number of dynamical DE models, and an analytical approximation for it, to be used to set the initial conditions of N-body simulations.

Using these formulae, we modified the ART code, which is used in the accompanying paper (Klypin et al. 2003). In a similar way, other programs dealing with N-body interactions or hydrodynamics can be appropriately modified.

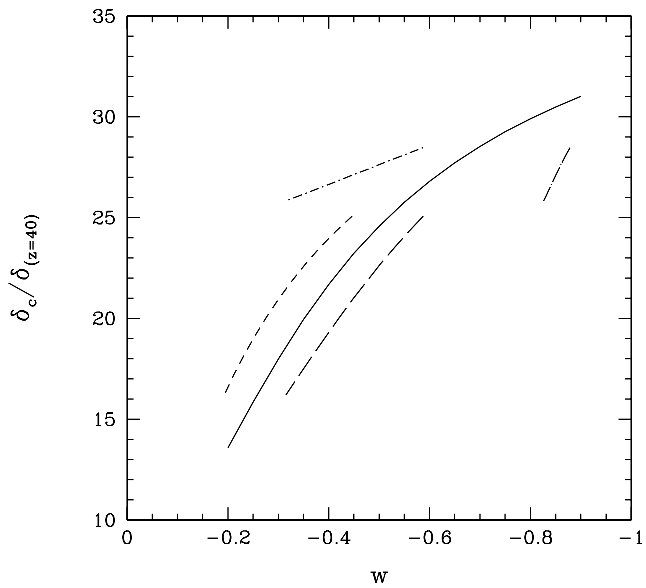

FIG. 10.—Linear growth factor for models with $w =$ const (*solid curve*) compared with the linear growth factor for the RP and SUGRA models (*dashed and dot-dashed curves, respectively*). The RP and SUGRA results are plotted as a function of the value of w that they have at either $z = 0$ or $z = 40$ (*long-dashed and short-dashed lines, respectively*). The logarithmic energy scale λ for both models ranges here from 2 to 10. The plot illustrates that the growth factor for dynamical DE cannot be easily approximated by any model with constant w.

REFERENCES

Balbi, A., et al. 2000, ApJ, 545, L1
Brax, P., & Martin, J. 2000, Phys. Rev. D, 61, 103502
Brax, P. H., & Martin, J. 1999, Phys. Lett. B, 468, 40
Brian, G., & Norman, M. 1998, ApJ, 495, 80
Caldwell, R. R. 2002, Phys. Lett. B, 545, 23
Coles, P., & Lucchin, F. 1995, Cosmology (New York: Wiley)
Dvali, G., & Turner, M. S. 2003, preprint (astro-ph/0301510)
Eke, V. R., Cole, S., & Frenk, C. S. 1996, MNRAS, 282, 263
Gott, J. R., III, & Rees, M. 1975, A&A, 45, 365
Gunn, J. E., & Gott, J. R., III 1972, ApJ, 176, 1
Klypin, A., Macciò, A. V., Mainini, R., & Bonometto, S. A. 2003, ApJ, 599, 31
Kravtsov, A., Klypin, A., & Khokhlov, A. 1997, ApJS, 111, 73
Lahav, O., Rees, M. J., Lilje, P. B., & Primack, J. R. 1991, MNRAS, 251, 128
Lokas, E. L. 2002, preprint (astro-ph/0112031)
Macciò, A. V., Murante, G., & Bonometto, S. A. 2003, ApJ, 588, 35
Mainini, R., Macciò, A. V., & Bonometto, S. A. 2003, NewA, 8, 173 (MMB03)
Netterfield, C. B., et al. 2002, ApJ, 571, 604
Peebles, P. J. E. 1980, The Large Scale Structure of the Universe (Princeton: Princeton Univ. Press)
Peebles, P. J. E., & Ratra, B. 2003, Rev. Mod. Phys., 75, 559
Perlmutter, S., et al. 1999, ApJ, 517, 565
Podariu, S., & Ratra, B. 2000, ApJ, 532, 109
Pogosyan, D., Bond, J. R., & Contaldi, C. 2003, in IAP Colloq. XVIII, The Nature of Dark Energy, ed. P. Brax, J. Martin, & J. P. Uzan (Paris: IAP), in press
Press, W. H., & Schechter, P. 1974, ApJ, 187, 425 (PS)
Ratra, B., & Peebles, P. J. E. 1988, Phys. Rev. D, 37, 3406 (RP)
Riess, A. G., et al. 1998, AJ, 116, 1009
Schuecker, P., Caldwell, R. R., Böhringer, H., Collins, C. A., & Guzzo, L., & Weinberg, N. N. 2003, A&A, 402, 53
Schulz, A. E., & White, M. 2001, Phys. Rev. D, 64, 043514
Sheth, R. K., & Tormen, G. 1999, MNRAS, 308, 119
———. 2002, MNRAS, 329, 61 (ST)
Spergel, D. N., et al. 2003, ApJS, 148, 175
Steinhardt, P. J., Wang, L., & Zlatev, I. 1999, Phys. Rev. D, 59, 123504
Tegmark, M., Zaldarriaga, M., & Hamilton, A. J. 2001, Phys. Rev. D, 63, 43007
Wang, L., & Steinhardt, P. J. 1998, ApJ, 508, 483
Wetterich, C. 1988, Nucl. Phys. B, 302, 668
Zlatev, I., Wang L., & Steinhardt, P. J. 1999, Phys. Rev. Lett., 82, 896